

**SPARC-GE-04/003**  
**17 September 2004**

## **CONTRIBUTIONS TO FEL 2004**

(29 August-3 September 2004, Trieste, Italy)

- 1) Status Report on Sparc Project
- 2) The Sparx Project: R&D Activity Towards X-Rays FEL Sources
- 3) Spectral Analysis of Charge Emission Spatial Inhomogeneities and Emittance Dilution in RF Guns
- 4) Harmonic Generation and Linewidth Narrowing in Seeded FELs
- 5) Seeding High Gain Harmonic Generation with Laser Harmonics Produced in Gases

# STATUS REPORT ON SPARC PROJECT

A. Renieri\*, M. Carpanese, F. Ciocci, G. Dattoli, A. Di Pace, A. Doria, F. Flora, G.P. Gallerano, L. Giannessi, E. Giovenale, G. Messina, L. Mezi, P.L. Ottaviani, S. Pagnutti, G. Parisi, L. Picardi, M. Quattromini, G. Ronci, C. Ronsivalle, E. Sabia, M. Sassi, A. Zucchini, ENEA, Centro Ricerche Frascati, C.P. 65, 00044 Frascati, Italy

D. Alesini, M. Bellaveglia, S. Bertolucci, M.E. Biagini, C. Biscari, R. Boni, M. Boscolo, M. Castellano, A. Clozza, G. Di Pirro, A. Drago, A. Esposito, M. Ferrario, D. Filippetto, V. Fusco, A. Gallo, A. Ghigo, S. Guiducci, M. Incurvati, C. Ligi, F. Marcellini, M. Migliorati, C. Milardi, L. Palumbo, L. Pellegrino, M. Preger, P. Raimondi, R. Ricci, C. Sanelli, M. Serio, F. Sgamma, B. Spataro, A. Stecchi, A. Stella, F. Tazzioli, C. Vaccarezza, M. Vescovi, C. Vicario, M. Zobov, INFN-Frascati, Italy

F. Alessandria, A. Bacci, I. Boscolo, F. Broggi, S. Cialdi, C. De Martinis, D. Giove, C. Maroli, V. Petrillo, M. Romè, L. Serafini, INFN-Milano, Italy

D. Levi, M. Mattioli, G. Medici, P. Musumeci, INFN-Roma1, Roma, Italy

L. Catani, E. Chiadroni, S. Tazzari, INFN-Roma2, Roma, Italy

C.J. Bocchetta, M. Danailov, G. D'Auria, M. Ferianis, Elettra, Trieste, Italy

A. Cianchi, A. D'Angelo, R. Di Salvo, A. Fantini, D. Moricciani, C. Schaerf, Università di Roma Tor Vergata, Roma, Italy

S. Reiche, J.B. Rosenzweig, G. Travish, UCLA, Los Angeles, CA, USA

D.H. Dowell, P. Emma, C. Limborg, D. Palmer, SLAC, Stanford, CA, USA

## Abstract

We review the status of FEL source activity of the ongoing SPARC FEL experiment, developed within the framework of a collaboration among ENEA, CNR, INFN, INFN, Sincrotrone Trieste and University of Rome Tor Vergata. The project is aimed at realising a SASE-FEL source, operating in the visible (around 500 nm), with an extended range of tunability down to the VUV (100 nm) by the use of the mechanism of non-linear harmonic generation. The development of the relevant activities foresees the realisation of an advanced 150 MeV photoinjector source, aimed at producing a high brightness electron beams, needed to drive a SASE-FEL experiment, and a 14 m long undulator. We present the status of the design and construction of SPARC FEL device. In particular we discuss the choice of the project parameters, their optimisation and the sensitivity of the SPARC performance to any parameter variation. We will show, using start-to-end simulations, what is the impact of the e-beam and of the undulator parameters on the characteristics of the output laser field and in particular on the amount of the non-linearly generated power at higher harmonics.

## INTRODUCTION

The *SPARC* project, funded by the Italian Government in 2003 with a 3 year time schedule, is an R&D activity aimed to develop a high brightness photoinjector for self-amplified spontaneous emission free-electron laser (SASE-FEL) experiments. The installation of the machine at LNF will start on September 2004, and the first beam is expected on June 2006. The SPARC [1] complex is composed of an RF gun driven by a Ti:Sa laser producing 10 ps flat top pulses that hit on a photocathode. The outgoing beam is injected into three SLAC accelerating sections to feed a 14 m long undulator (Fig. 1).



Figure 1: SPARC project layout.

\* Renieri@frascati.enea.it

The main goals of the project are:

1. the generation of a high brightness electron beam able to drive a SASE-FEL experiment in the green visible light and higher harmonics generation;
2. the development of an ultra-brilliant beam photoinjector needed for the future SASE-FEL based X-ray sources.

## WORKING POINT OPTIMIZATION

The beam current required by the FEL experiment pushes the injector design towards the limits of the state-of-the-art for what concerns pulse charge and pulse shape. The design goal of the SPARC accelerator is to provide a 155 MeV bunch with projected emittance lower than 2  $\mu\text{m}$  and slice emittance lower than 1  $\mu\text{m}$ . The SPARC FEL operates in the diffraction dominated range and peak current is a key parameter for shortening the FEL gain length. Once including possible errors in the undulator system (see next section), the analysis of the SPARC FEL operation shows that, in order to leave a significant contingency margin to ensure full saturation and testing of harmonic generation, a safer parameter set requires a beam having 100 A in 50% of the slices with a slice emittance  $\leq 1 \mu\text{m}$ . For this purpose a new optimization was performed, with start-to-end simulations and parametric sensitivity studies aiming to reduce the FEL saturation length. The best result was obtained with a scaling approach [2] in which more charge is launched from the cathode. The configuration that gives the minimum emittance corresponds to a working point with 1.1 nC and a pulse length of 10 ps. The overall result is the reduction of the SASE-FEL saturation length from 12 to 9 m at 500 nm wavelength. The beam characterization is shown in Fig. 2, while FEL power as a function of  $z$  as obtained with the GENESIS code is reported in Fig. 3. In Tab. 1 and 2 the final parameter sets are reported.

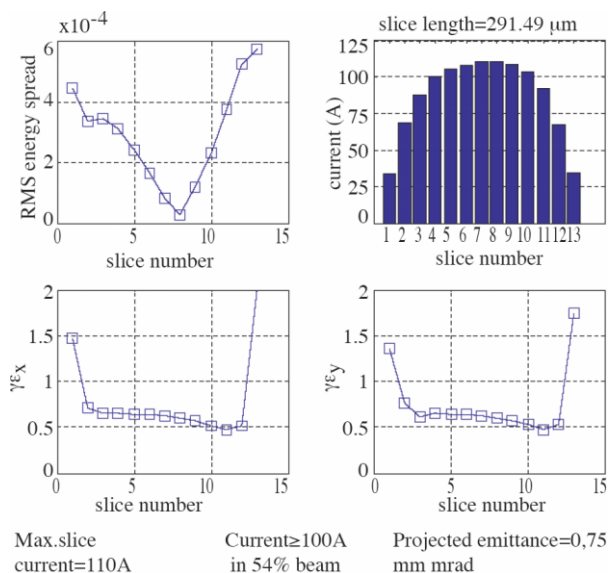


Figure 2: “Slice” electron beam energy spread, peak current,  $x$  and  $y$  emittances (PARMELA code).

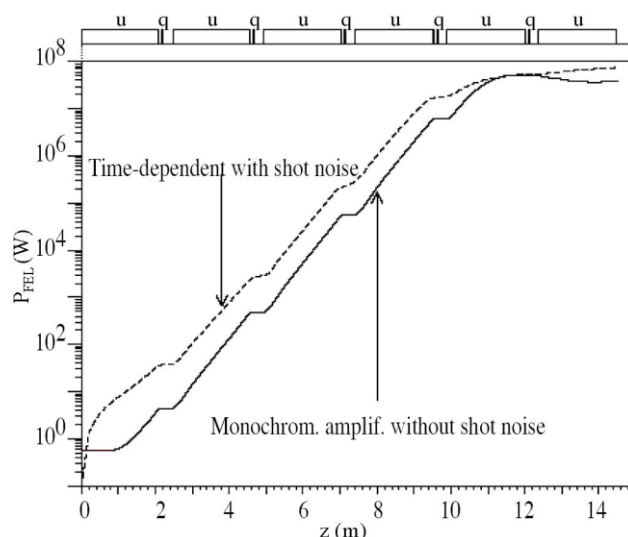


Figure 3: FEL power longitudinal evolution ( $\lambda_u = 2.8 \text{ cm}$ ,  $K = 2.1413$ ,  $I = 110 \text{ A}$ ).

Table 1: Injector parameters.

ELECTRON BEAM	
Electron beam energy (MeV)	155
Bunch charge (nC)	1.1
Repetition rate (Hz)	1-10
Cathode peak field (MV/m)	120
Peak solenoid field @ 0.19 m (T)	0.273
Laser spot size, hard edge radius (mm)	1.13
Central RF launch phase (deg)	33
Laser pulse duration, flat top (ps)	10
Laser pulse rise time 10% $\rightarrow$ 90% (ps)	1
Bunch energy @ gun exit (MeV)	5.6
Bunch peak current @ linac exit (A)	100
RMS normalized transverse emittance @ linac exit (mm-mrad); includes thermal comp. (0.3)	< 2
RMS slice norm. emittance (300 $\mu\text{m}$ )	< 1
RMS longitudinal emittance (deg.keV)	1000
RMS total correlated energy spread (%)	0.2
RMS uncorrelated energy spread (%)	0.06
RMS beam spot size @ linac exit (mm)	0.4
RMS bunch length @ linac exit (mm)	1

Table 2: FEL parameters.

UNDULATOR & FEL	
Undulator period (cm)	2.8
No. of undulator sections	6
Undulator parameter	2.16
Undulator field on axis (T)	0.83
Undulator gap (mm)	9.25
Undulator section length (m)	2.13
Drifts between undulator sections (m)	0.36
FEL wavelength (nm)	500
Saturation length, geometrical (m)	< 14
FEL pulse length (ps)	8
FEL power @ saturation (MW)	> 80
No. of photons/pulse	$10^{15}$
FEL power @ saturation, 3 <sup>rd</sup> harm. (MW)	> 10
FEL power @ saturation, 5 <sup>th</sup> harm. (MW)	> 0.7

The SPARC project foresees the possibility of extending the tunability range by exploiting the non-linear generation of higher order harmonics. The understanding of the mechanism underlying such a process has required a strong effort involving analytical and numerical means [3] and, as to the SPARC proposal, it has been shown that it is possible to obtain a significant amount of coherent power at higher order harmonics, which guarantees a brightness of third (170 nm) and fifth (100 nm) harmonic two orders of magnitude only below the fundamental.

## UNDULATOR SYSTEM

In this type of FEL one of the most significant problems is that of reaching a good level of mechanical precision along the whole length of the undulator, which is a flexible structure. It is therefore evident that one of the first effects to be included in the optimization of the device is that of bending of the undulator section due to the magnetic and gravitational forces (Fig. 4). The variations of the longitudinal profile will be in turn responsible of magnetic field variations, which will provide a kind of inhomogeneous broadening and thus a gain reduction along with an increase of the saturation length.

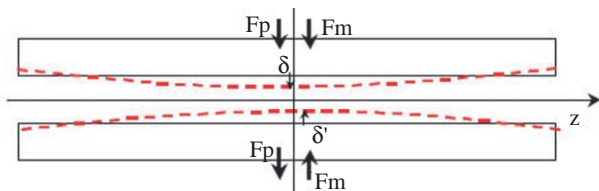


Figure 4: Flexure of the undulator upper and lower faces induced by the attractive magnetic forces and the gravity.

The problem of understanding the undulator bending effects on the SASE-FEL dynamics has been considered by merging two different points of view:

- a typical engineering approach [4], according to which we have defined the maximum bending as a function of the attractive forces and of the Young modules of the relevant materials;
- a method based on dynamical simulations [5][6], which have been able to evaluate the effects of a given flexure on the laser performances.

An example of the effects due to the profile variations on the final laser power and on the subharmonics is given in Fig. 5, which shows how such an effect may become significant for values of the maximum deflection above 10  $\mu\text{m}$ . This example yields just an idea of the problems arising within the study of the optimization of the device. There are indeed other effects which cannot be considered by their own and should be combined with the others, as e. g. those associated with the fact that the surface of the undulator poles assembly may not be perfectly parallel.

This fact may combine with possible misalignments between undulator sections and it may induce a further gain reduction (Fig. 6), which has been accurately modelled [6].

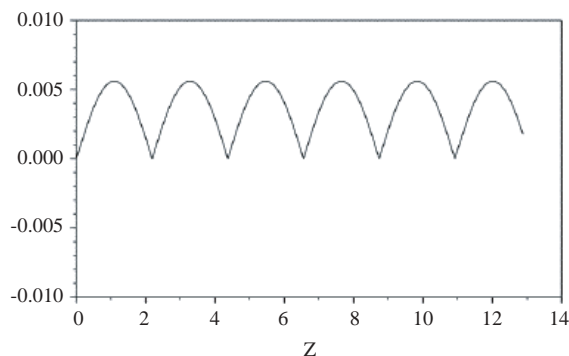


Figure 5a: Longitudinal on axis field variation along the six undulator sections due to the induced flexure.

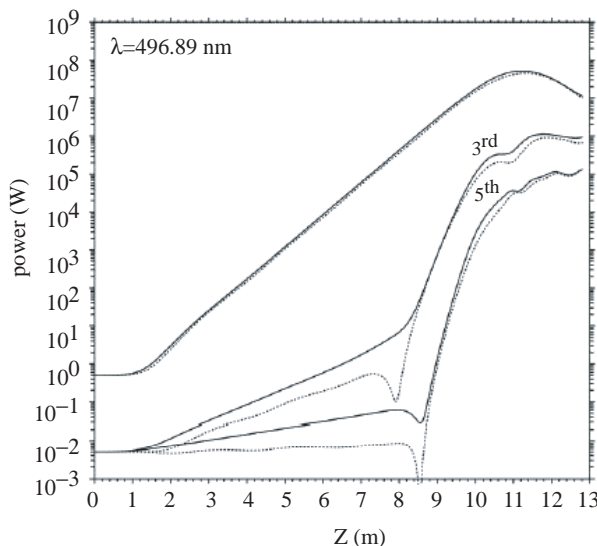


Figure 5b: Effect of the induced flexure on the power evolution of the fundamental and higher order harmonics (solid: no flexure, dots: 10  $\mu\text{m}$  maximum flexure in the centre; Prometeo code).

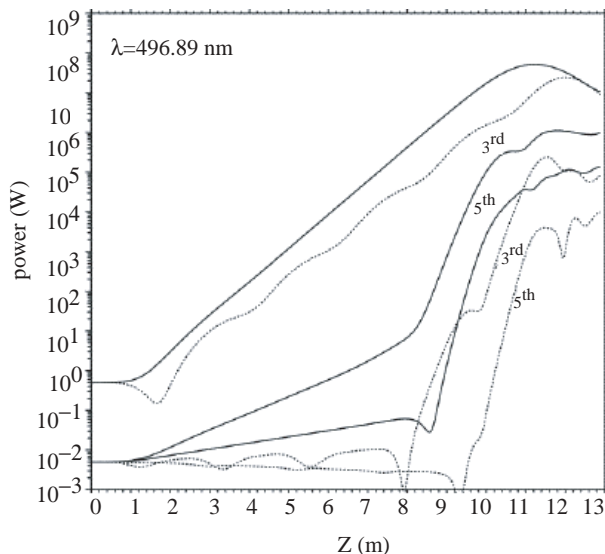


Figure 5c: As in Fig. 5b for 50  $\mu\text{m}$  maximum flexure (Prometeo code).

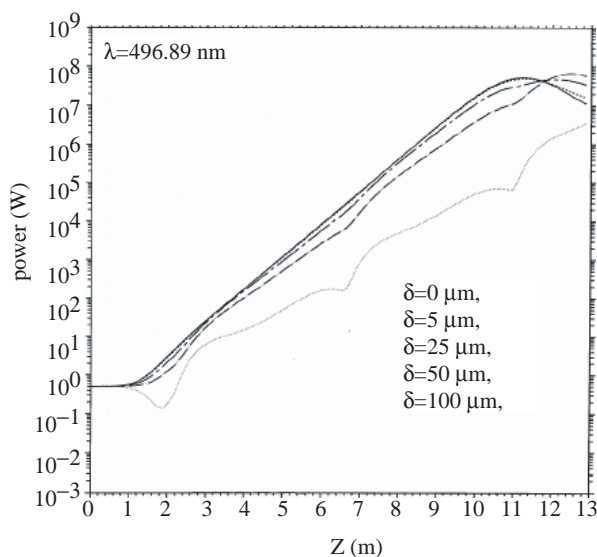


Figure 6: Effect of undulator faces misalignment on the laser power for different values of the maximum flexure  $\delta$  (Prometeo code).

## OPTICAL DIAGNOSTICS

The diagnostic layout is shown in Fig. 7; a diagnostic chamber is positioned in correspondence of each undulator section. Through these chambers the FEL radiation is extracted and transported up to a measurement station placed at the ending part of the FEL.

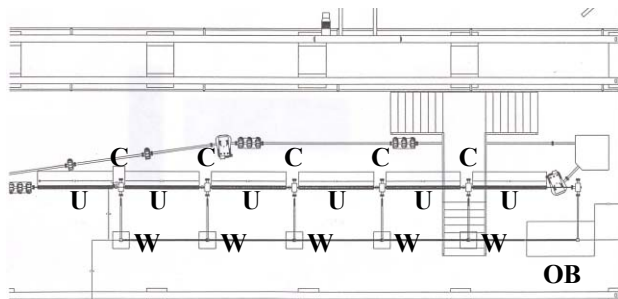


Figure 7: Diagnostic layout. U: undulator sections; C: diagnostic chambers; W: workstations for the analysis of the radiation from each undulator; OB: optical bench.

The study and the design of the diagnostic chamber foresee a series of conditions to be fulfilled. Among them the most significant one is due to the reduced space available for its installation. The distance between the different undulator sections is about 36 cm and within such a space it will be necessary to allocate, along with the diagnostic chamber, the quadrupoles for the electron focusing on the horizontal plane. The schematic layout of the diagnostic chamber is shown in Fig. 8. The diagnostic chamber will host “pop-up” mirrors to extract the FEL radiation as well as electron diagnostics, alignment screens based on transition radiation and all necessary ports to connect to the vacuum pumping system.

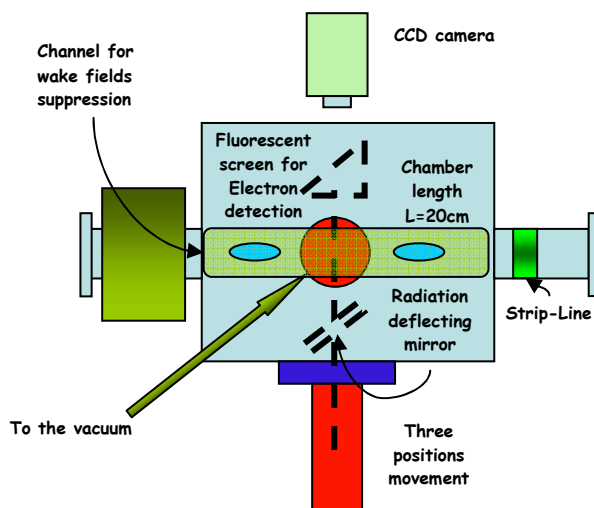


Figure 8: Diagnostics chamber.

A non-interceptive diagnostics, which will be tested at a later stage of the SPARC project, is based on the interaction between the electron beam and a metal grating. It has been shown that such a device is capable of providing quantitative information about the longitudinal bunch profile from the power spectrum of the emitted coherent spontaneous radiation [7].

## CONCLUSIONS

The SPARC project has been approved by the Italian Government and funded in June 2003 with a schedule of three years. After the first year the project has been fully defined and the major components have been ordered.

## REFERENCES

- [1] SPARC Project Team, “SPARC Injector TDR”, ([www.inf.infn.it/acceleratori/sparc](http://www.inf.infn.it/acceleratori/sparc)).
- [2] J.B. Rosenzweig and E. Colby, “Advanced Accelerator Concepts”, AIP Conf. Proc. 1995, Vol. 335, p. 724.
- [3] G. Dattoli, L. Giannessi, P.L. Ottaviani and A. Torre, J. Appl. Phys. (2004); G. Dattoli, these proceedings.
- [4] A. Zucchini, “Considerazioni relative alla flessione del supporto e dei magneti a causa del campo magnetico”, SPARC Tech. Note 03/007 ([www.sparc.it](http://www.sparc.it)).
- [5] F. Ciocci, G. Dattoli, L. Mezi and P.L. Ottaviani, “The effect of the magnetic deflection on the FEL evolution: a dynamical point of view”, SPARC Tech. Note 03/005 ([www.sparc.it](http://www.sparc.it)).
- [6] F. Ciocci, G. Dattoli, L. Mezi and P.L. Ottaviani, “Angular Tolerances in the SPARC undulator”, SPARC Tech. Note 03/008 ([www.sparc.it](http://www.sparc.it)).
- [7] G. Doucas, M.F. Kimmitt, A. Doria, G.P. Gallerano, E. Giovenale, G. Messina, H.L. Andrews, J.H. Brownell, “Determination of longitudinal bunch shape by means of coherent Smith-Purcell radiation”, Phys. Rev. Special Topics – Accelerators and Beams Vol. 5, 072802 (2002).

# THE SPARX PROJECT: R&D ACTIVITY TOWARDS X-RAYS FEL SOURCES

D.Alesini, S.Bertolucci, M. Bellaveglia, M.E.Biagini, R.Boni, M.Boscolo, M.Castellano, A.Clozza, G.Di Pirro, A.Drago, A.Esposito, M.Ferrario, D. Filippetto, V.Fusco, A.Gallo, A.Ghigo, S.Guiducci, M.Incurvati, C.Ligi, F.Marcellini, M.Migliorati, A.Mostacci, L.Palumbo, L.Pellegrino, M.Preger, P. Raimondi, R.Ricci, C.Sanelli, M.Serio, F.Sgamma, B.Spataro, A.Stecchi, A.Stella, F.Tazzioli, C.Vaccarezza, M.Vescovi, C.Vicario, INFN-Frascati

F.Alessandria, A.Bacci, I.Boscolo, F.Broggi, S.Cialdi, C.De Martinis, D.Giove, C.Maroli, M. Mauri, V.Petrillo, M.Rome, L.Serafini, INFN-Milano

M.Mattioli, P. Musumeci, INFN-Roma1

L.Catani, E.Chiadroni, A. Cianchi, C. Schaerf, INFN-Roma2

F.Ciocci, G.Dattoli, A. Di Pace, A.Doria, F.Flora, G.P.Gallerano, L.Giannessi, E.Giovenale, G.Messina, L.Mezi, P.L.Ottaviani, S. Pagnutti G. Parisi, L.Picardi, M.Quattromini, A.Renieri, C.Ronsivalle, A. Torre, A. Zucchini, ENEA-Frascati

S. De Silvestri, M. Nisoli, S. Stagira, Politecnico/Milano

J.B. Rosenzweig, S. Reiche, UCLA - Dept. of Physics and Astronomy

P.Emma, SLAC

## *Abstract*

SPARX is an evolutionary project proposed by a collaboration among ENEA-INFN-CNR-Universita' di Roma Tor Vergata aiming at the construction of a FEL-SASE X-ray source in the Tor Vergata Campus. The first phase of the SPARX project, funded by Government Agencies, will be focused on R&D activity on critical components and techniques for future X-ray facilities as described in this paper.

## INTRODUCTION

SPARX is an evolutionary project proposed by a collaboration among ENEA-INFN-CNR-Universita' di Roma Tor Vergata aiming at the construction of a FEL-SASE X-ray source in the Tor Vergata Campus. The first phase of the SPARX project, funded by Government Agencies with 10 Million Euro plus a preliminary contribution of 2.35 Million Euro by INFN, will be focused on R&D activity on critical components and techniques for future X-ray facilities. A R&D program towards a high brightness photoinjector (SPARC project [1]) is already under way at LNF-INFN. Its aim is the generation of electron beams with ultra-high peak brightness to drive a SASE-FEL experiment at 500 nm, performed with a 14 m long undulator [2]. The R&D plans for the X-ray FEL source will be developed along two lines: (a) use of the SPARC high brightness photoinjector to develop experimental test on RF compression

techniques and other beam physics issues, like emittance degradation in magnetic compressors due to CSR, (b) explore production of soft and hard X-rays in a SASE-FEL with harmonic generation, in the so called SPARXINO test facility, upgrading in energy and brightness the existing Frascati 800 MeV Linac at present working as injector for the DAΦNE  $\phi$ -factory (Fig. 1).



Figure 1: View of the Frascati linac

A parallel program will be aimed at the development of other critical component for X-rays FEL sources like high repetition rate S-band gun, high Quantum Efficiency cathodes, high gradient X-band RF accelerating structures

and harmonic generation in gas. In the next sections we describe preliminary start to end simulations for the SPARXINO test facility, the required R&D efforts and a possible solution for the DAΦNE linac upgrade.

## THE SPARXINO TEST FACILITY

The spectral range from 10 nm to 1 nm, has been considered for the radiation source. In order to generate the SASE-FEL in this wavelength range, it is necessary to produce a high brightness beam to inject inside the undulators. A preliminary analysis of the beam parameters required for such a source leads to the values reported in Tab. 1.

Table 1: Electron beam parameter

Beam Energy	1	GeV
Peak current	2	kA
Emittance (average)	2	mm-mrad
Emittance (slice)	1	mm-mrad
Energy spread (correlated)	0.1	%

The basic scheme is shown in Fig. 2 and consists of an advanced high brightness photoinjector followed by a first linac driving the beam up to 350 MeV with the correlated energy spread required to compress it in a following magnetic chicane. The second linac drives the beam up to 1 GeV while damping the correlated energy spread taking profit of the effective contribution of the longitudinal wake fields provided by the S-band accelerating structures.

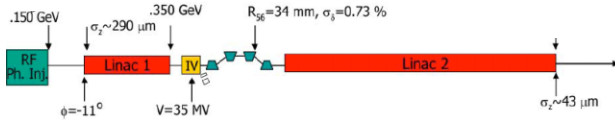


Figure 2: Scheme of the SPARXINO test facility.

A peculiarity of this linac design is the choice to integrate a rectilinear RF compressor in a high brightness photoinjector, as proposed in [3], thus producing a 300-500 A beam in the early stage of the acceleration. The SPARXINO linac will be the first SASE FEL experiment operating with RF and magnetic compressors in the same linac. The potentially dangerous choice to compress the beam at low energy (<150 MeV) when it is still in the space charge dominated regime, results from simulations not too difficult provided a proper emittance compensation technique is adopted [4], a possibility that is not viable in a magnetic chicane. In addition the propagation of a shorter bunch in the first linac reduces the potential emittance degradation caused by transverse wake fields and longitudinal wake fields result to be under control by a proper phasing of the linac. A comparison between the two compression techniques is scheduled during the SPARC phase II operation.

The preliminary design of the injector for the SPARXINO test facility is a copy of the SPARC high brightness photoinjector [1]. It considers a 1 nC bunch 10 ps long (flat top) with 1 mm radius, generated inside a 1.6-cell S-band RF gun of the same type of the BNL-SLAC-UCLA one [5] operating at 120 MV/m peak field equipped with an emittance compensating solenoid. Three standard SLAC 3-m TW structures each one embedded in a solenoid boost the beam up to 150 MeV.

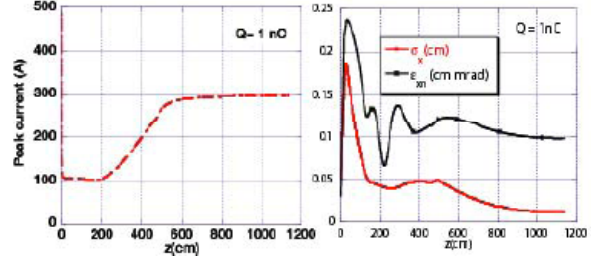


Figure 3: rms current (left), rms norm. emittance and rms beam envelope (right) along the injector, up to 150 MeV.

With a proper setting of the accelerating section phase and solenoids strength it is possible to increase the peak current preserving the beam transverse emittance. In the present case we have got with PARMELA simulation a bunch average current of 300 A with a normalized rms emittance below 1 mm-mrad.

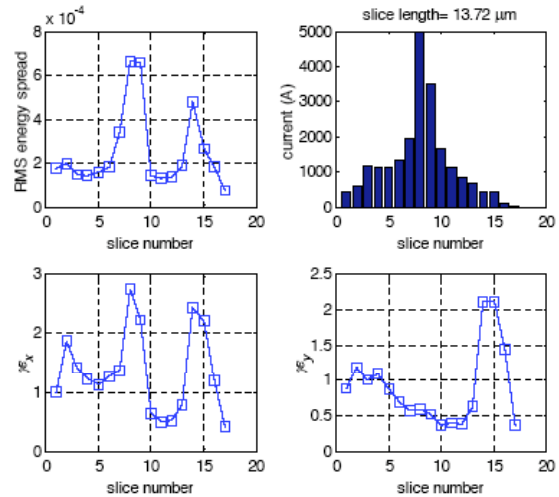


Figure 4: Energy spread, peak current and transverse emittances along the bunch, at the linac exit.

The low compression ratio (a factor 3) has been chosen to keep the longitudinal and transverse emittances as low as possible in order to simplify the second compression stage. We used the first two TW sections as compressor stages in order to achieve a gradual and controlled bunching, the current has to grow at about the same rate of the energy, and we increased the focusing magnetic field during the compression process. Fig. 3 (left) shows the current growth during bunch compression until 150 MeV, envelope and emittance evolution are also reported

(right), showing the emittance compensation process driven by the solenoids around the accelerating section that keep the bunch envelope close to an equilibrium size during compression.

The 10k macro-particles beam generated by PARMELA [6] has been propagated through Linac1, Magnetic Compressor and Linac2 with the code ELEGANT [7]. The correlated energy spread induced by Linac1 is 0.7% in order to compress the beam by a factor 6 in the 10 m long magnetic chicane with  $R_{56} = 34$  mm. At the exit of Linac2 the required parameters for FEL operation have been achieved over more than 30% of the bunch length, as shown in Fig. 4. A further improvement is expected by fully optimizing the compression scheme and by using a 4<sup>th</sup> harmonic cavity [8] for the linearization of the longitudinal phase space distribution

## THE SASE FEL SOURCE

Time dependent FEL simulations, performed with the code GENESIS [9] using the particle distributions produced by the Linac simulations presented in the previous section are in progress showing saturation for 30% of bunch slices after 16 m of active undulator length. We assume to use the same undulator of the SPARC project [2] with two additional 2.13 m long modules required to saturate at 10 nm, see Fig. 5. These first preliminary results are encouraging and will be the starting point for further optimizations

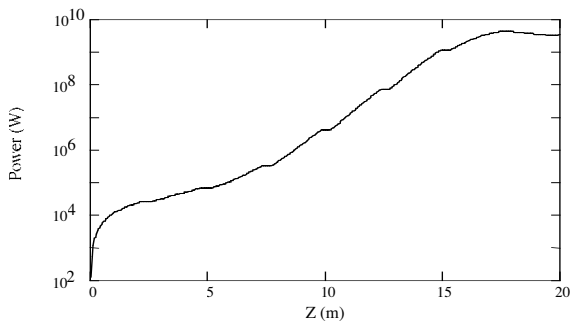


Figure 5: Power vs. z for the 10 nm SPARXINO SASE-FEL source, GENESIS simulation (slice energy spread  $8 \cdot 10^{-4}$ , slice norm. emittance 1 mm mrad, slice peak current 2 kA, undulator parameter  $K=2.2$ )

## DAΦNE LINAC UPGRADE

The DAΦNE injection system is a 60 m long LINAC equipped with 15 S-band (2.865 GHz) SLAC-type 3 m long accelerating structures driven by four 45 MW klystrons each followed by a SLED peak power doubling system. At present it delivers 0.8 μs RF pulses at a repetition rate of 50 Hz as required for DAΦNE operation. A quadrupole FODO focusing system is distributed along the entire linac. It accelerates the positron bunches emerging by the Positron Converter, up to the maximum energy of 550 MeV and the electron bunches up to 800 MeV. A drift space of about 15 m is

available at the linac output for the installation of the undulator.

The Linac energy upgrade to 1 GeV can be achieved, as shown in figure 6, by pushing the accelerating field of the existing units up to 26 MV/m, which is today easily attainable and by adding 2 new SLAC-type sections to reach 1.1 GeV. The Linac waveguide network must also be modified in order to supply two accelerating units per RF station. This system configuration requires two new 45 MW klystrons.

High beam brightness can be achieved by installing a copy of the 12 m long SPARC photoinjector upstream the DAFNE linac with a minor modification of the existing building and a magnetic compressor at 350 MeV in the area of the Positron Converter, thus keeping the possibility to operate the linac as DAΦNE injector. A detailed analysis of the SPARXINO test facility compatibility with the proposed DAΦNE energy upgrade operation is under way [10].

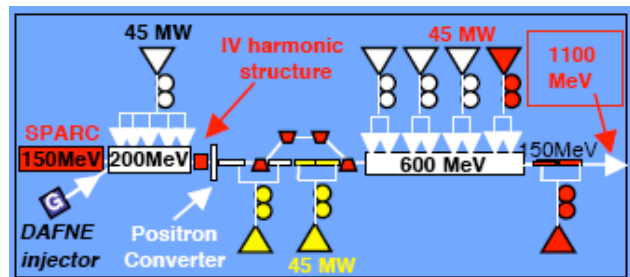


Figure 6: Scheme of the Frascati linac upgrade for SPARXINO and DAΦNE operation. Existing elements (white). Additional SPARXINO elements (red). Additional elements for positron acceleration (yellow).

## CONCLUSIONS

The SPARX R&D project has been approved by the Italian Government and funded in June 2004 with a schedule of three years. The critical components for an X-ray FEL source will be tested during phase II of the SPARC project and assembled in a high energy and high brightness linac, the SPARXINO test facility, by upgrading the existing Frascati linac.

## REFERENCES

- [1] SPARC Project Team, Sparc Injector TDR [www.lnf.infn.it/acceleratori/sparc/](http://www.lnf.infn.it/acceleratori/sparc/)
- [2] A. Renieri et al., "Status Report on SPARC Project", this conference.
- [3] L. Serafini and M. Ferrario, Velocity Bunching in PhotoInjectors, AIP CP 581, 2001, pag.87
- [4] M. Boscolo et al., Beam Dynamics Study of RF Bunch Compressors for High Brightness Beam Injectors, Proc. of EPAC 2002, Paris.
- [5] D.T. Palmer, The next generation photoinjector, PhD. Thesis, Stanford University
- [6] J. Billen, "PARMELA", LA-UR-96-1835, 1996.

- [7] M. Borland, "elegant: A Flexible SDDS-Compliant Code for Accelerator Simulation" LS-287, ANL, Argonne, IL 60439, USA.
- [8] A. Bacci, M. Migliorati, L. Palumbo, B. Spataro, "An X-Band structure for a longitudinal emittance correction at Sparc", LNF - 03/008 (R), and D. Alesini, A. Bacci, M. Migliorati, A. Mostacci, L. Palumbo, B. Spataro: "Studies on a Bi-Periodic X-Band Structure for SPARC", LNF-03-013(R).
- [9] S. Reiche, Nucl. Instrum. & Meth. A429,243 (1999).
- [10] R. Boni, "Feasibility of the DAFNE-Linac energy doubling", Proc. of the Workshop on e+e- in the 1-2 GeV range, Alghero, Italy, September 2003

# SPECTRAL ANALYSIS OF CHARGE EMISSION SPATIAL INHOMOGENEITIES AND EMITTANCE DILUTION IN RF GUNS

M. Quattromini, L. Giannessi, C. Ronsivalle,  
ENEA, C.R. Frascati, Via E. Fermi, 45  
I - 00044 Frascati (Rome), Italy.

## Abstract

The effects of fluctuations in cathode's quantum efficiency and other sources of dis-homogeneities in the performances of a typical RF photo-injector have been investigated with PARMELA and TREDI numerical codes. The RF gun layout includes a focusing solenoid in a configuration aimed at minimizing the emittance growth due to space charge effects.

## INTRODUCTION

Many applications from X-ray Free electron lasers to high energy colliders require high brightness beams produced by photo-injectors. The final performances of these devices are strictly linked to the beam quality produced by the electron source. In the case of FELs the role played by emittance becomes crucial at sub-nm wavelengths where the emittance is related to the transverse coherence of the output radiation. Most of the emittance budget that characterizes the beam at the undulator is produced at the injector in the first stages of the beam acceleration. The emittance optimization procedure rely on the linear theory[1] which has been verified both experimentally and numerically. In this paper we extend the analysis presented in Ref.[2] where the role played by a non uniform electron emissivity was examined. This study has been performed by using two different codes based on different algorithms: the Los Alamos version of PARMELA (PARMELA-LANL)[3] and TREDI[4]. TREDI has been used in "static" mode, i.e. ignoring effects associated to the finite velocity propagation of signals within the bunch.

## PROBLEM DESCRIPTION

The aim of this work is to study the effect of charge in-homogeneities at the cathode surface, by decoupling in a transverse Fourier space, the in-homogeneities occurring at a specific wave-number , on a scale of the beam spot radius  $R$ , and higher. We have considered a standard S-Band (2856 MHz). 1.6 cells, BNL type photo-injector configuration[5], in a set-up optimized at minimizing the emittance in terms of accelerating gradient, extraction phase, beam spot size, focusing solenoid strength. Space charge effects compensation is achieved assuming both transverse and longitudinal flat charge distribution at extraction. The gun starts at  $z=0$  and the drifts ends at  $z=2$  m. The peak electric field in the gun and the solenoid peak magnetic field have been set respectively to 120 MV/m and 2.73 kG. The longitudinal shape of the pulse is square with

a length of 10 ps and the charge is 1 nC. The phase of the centre of the bunch is  $35^\circ$ . No thermal emittance is included. The beam spot radius  $R$  is 1 mm. In Ref.[2] the charge distribution extracted from the cathode was modelled as a perturbation with respect to the ideal case with the following cosine function showing a maximum on the centre of the spot:

$$\rho_p(x, y) = \rho_0 [1 + \delta \cdot \cos(k_n x)] [1 + \delta \cdot \cos(k_n y)] \quad (1)$$

for

$$x^2 + y^2 \leq R^2 \quad \text{and} \quad k_n = n \frac{2\pi}{R}$$

In this contribution we analyze the effect of a sin-like (odd) perturbation of the type

$$\rho_p(x, y) = \rho_0 [1 + \delta \cdot \sin(k_n x)] [1 + \delta \cdot \sin(k_n y)] \quad (2)$$

Assuming that the values of  $\delta$  and  $k_n$  are small, we may write in first approximation

$$\epsilon(k_n, \delta) = \epsilon_0 + \sum_n a_{n,j} \delta^j \quad (3)$$

where  $\epsilon_0$  is the value of the unperturbed emittance and the coefficients  $a_{n,j}$  show the sensitivity of the emittance in this injector configuration to the charge in-homogeneities at the frequency .

The study has been performed by varying the two parameters  $\delta$  and  $n$  and estimating the effect on the normalized rms emittance at the location of the first minimum (fig.1). The parameter  $\delta$  has been varied between 0 and 40% and  $n$  has been given the values  $n = 1/2, 1, 2, 4$ .

A previous comparison between codes in the ideal configuration, i.e. at  $\delta = 0$ , has shown a good agreement[6].

## RESULTS

The behaviour of the transverse emittance as a function of the longitudinal coordinate at  $\delta = 20\%$ , for different values of  $k_n$  is shown in figs. 1 and 2 for perturbed charge densities as of eqs. (1) and (2), respectively, as computed by TREDI. The emittance undergoes a typical series of oscillations due to the changes in correlation between longitudinal slices along the bunch which are subject to different focusing as a function of the extraction phase. These oscillations exhibit the well known structure with a double minimum located at the places where the correlation is maximized. In this analysis the second minimum does not appear since it falls behind the final longitudinal coordinate.

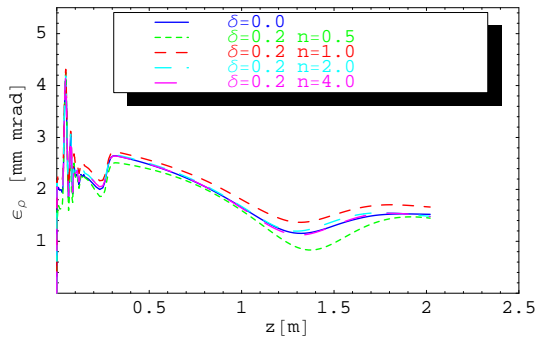


Figure 1: RMS transverse normalized emittance vs  $z$  for  $\delta = 20\%$  and  $n = 1/2, 1, 2, 4$  and perturbed density  $\rho$  as in eq. (1).

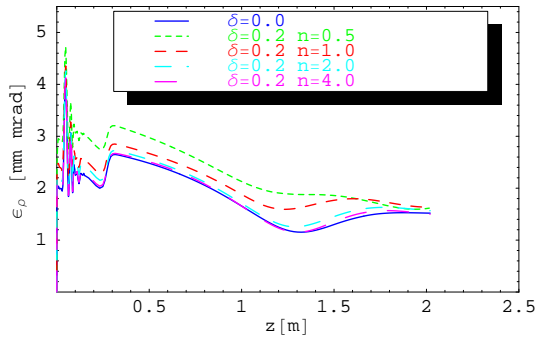


Figure 2: RMS transverse normalized emittance vs  $z$  for  $\delta = 20\%$  and  $n = 1/2, 1, 2, 4$  and perturbed density  $\rho$  as in eq. (2).

As an indication of the emittance of the beam we have considered the first minimum, whose position may depend on the in-homogeneity parameter  $\delta$  especially at the lower perturbation frequencies  $k_n$ . The effect of the asymmetry in perturbed density (2) induces clearly a much larger emittance dilution at lower values of the transverse “frequency”  $k_n$ . As expected, at higher frequencies, for the same value of  $\delta$ , the effect of different parity in charge distribution is negligible. In figure 3 the value computed by TREDI of the horizontal normalized rms emittance divided by the value obtained with a completely uniform distribution is plotted as a function of  $n$ . The data at  $n = 4$  may be affected by some aliasing. The transverse mesh size used to describe the space-charge fields is  $20 \times 20$  and could not be sufficient to resolve the fluctuations at  $n = 4$ . This may explain the slight emittance diminution observed in fig. 3. A more visible effect is predicted by TREDI for  $n = 0.5$  and  $\delta = 10\%$  (see fig. 4) for the charge distribution described by eq. (1). While this result is not evidenced by PARMELA, and require a further investigation, for  $n \geq 1$  the two codes are in fairly good agreement and both give the maximum emittance increase for  $n = 1$ . A possible explanation could be

related to the reduced transverse coupling of the beam with the RF photo-injector at the early stage of extraction[7].

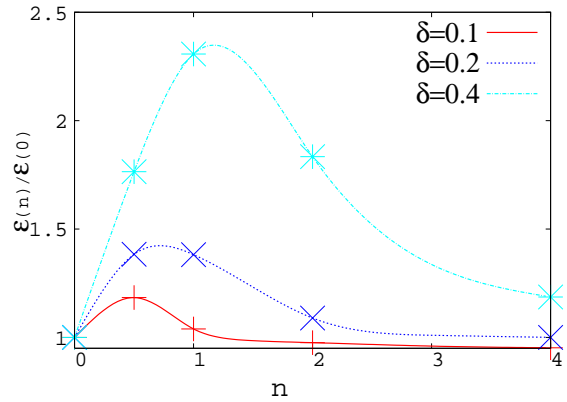


Figure 3: Emittance growth vs  $n$  in the position of the first minimum of the emittance as computed by TREDI for  $\rho$  as in eq. (2).

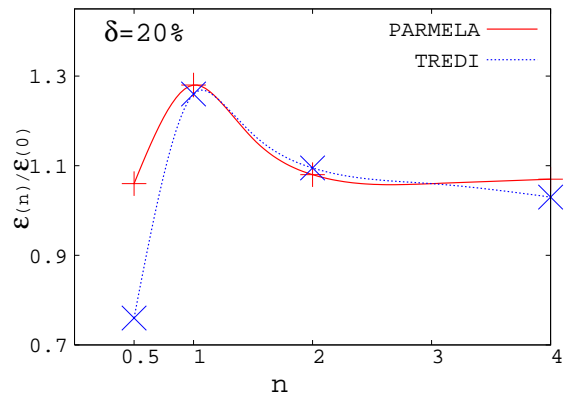


Figure 4: Emittance growth vs  $n$  in the first emittance minimum for  $\delta = 20\%$  as computed by PARMELA and TREDI for  $\rho$  as in eq. (1).

This behaviour may be understood by looking at the  $x$ - $y$  space shown in fig.5 in three longitudinal positions: at the cathode ( $z = 0$ ), near the minimum of emittance ( $z \approx 1.30$ m) and the local maximum of emittance ( $z \approx 1.5$ m). The non-linear space charge forces induced by the non uniform transverse distribution at the cathode give a deformation of the beam shape. The distortion is stronger when the non-uniformities are more localized respect to the cases in which they are more diffused and tend to a partial re-compensation along the drift.

In fig 5 the action of the solenoid focusing is also visible as a rotation of the distribution around the axis.

The emittance degradation increases with the modulation depth  $\delta$ , as expected. An analysis of the data similar to that performed in [2] yielded the same scaling law at high values of  $k_n$ . In fig 6 the result of a fit of  $\epsilon(\delta)/\epsilon_0$  for  $n = 2$  is shown. Clearly the function  $a_0 + a_3\delta^3$  fits the

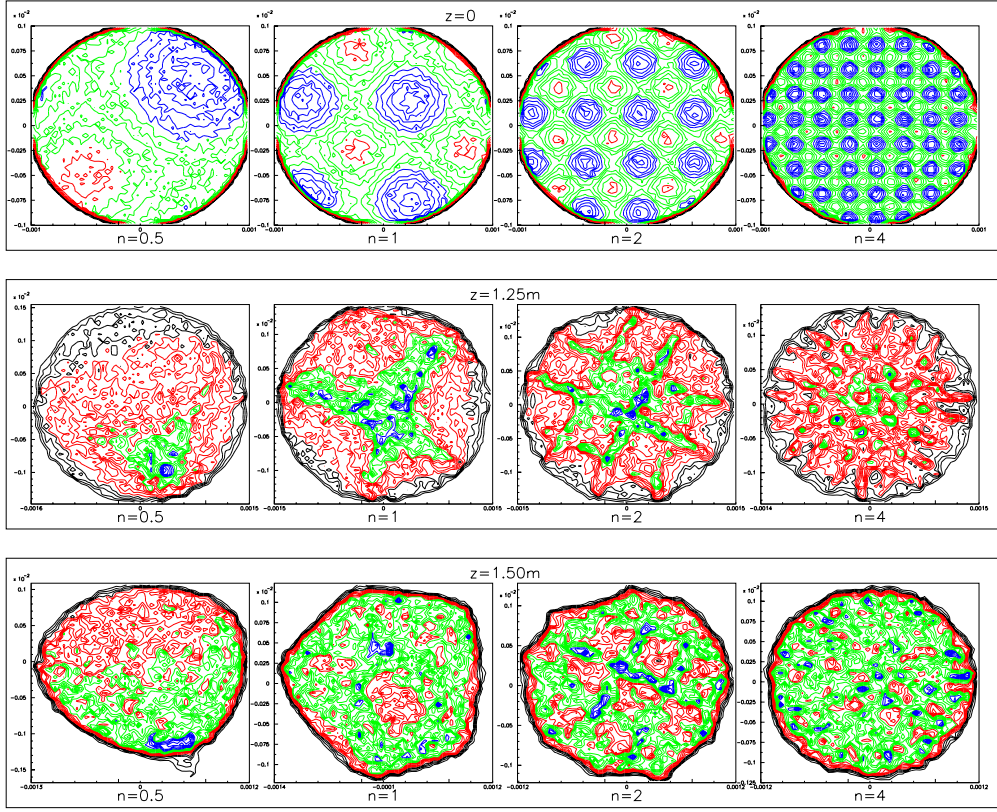


Figure 5: X-Y plots derived from TREDI computations for  $\delta = 20\%$  in different longitudinal positions for  $\rho$  as in eq. (2).

data better than  $a_0 + a_2\delta^2$ . By converse for  $n = 1$  (see fig 7) the quadratic law fits the data better than the cubic. This result is probably related to the asymmetry induced by the charge distribution (2) and is in agreement with the analysis developed in Ref. [8] where a quadratic scaling law was shown to reproduce well the emittance behaviour due to beam misalignments.

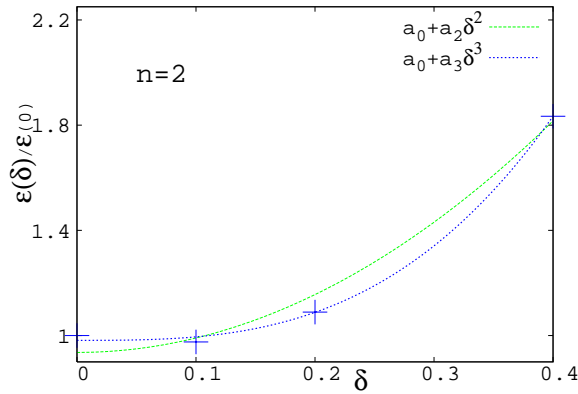


Figure 6: Emittance growth vs  $\delta$  for  $n = 2$  in the position of the first minimum of the emittance as computed by TREDI for  $\rho$  as in eq. (2).

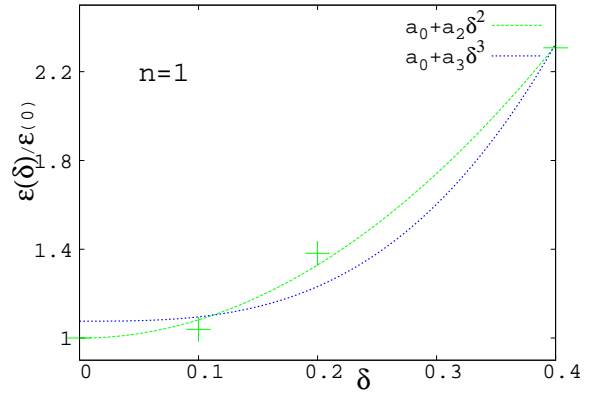


Figure 7: Emittance growth vs  $\delta$  for  $n = 1$  in the position of the first minimum of the emittance as computed by TREDI for  $\rho$  as in eq. (2).

## CONCLUSIONS

In this contribution we have extended the analysis of the emittance dilution as a function of the frequencies associated to a non axi-symmetric perturbation of the ideal transverse density extracted from the photocathode. A scaling law of this effect in function of the perturbation amplitude has been derived and some indications of the dependence of the effect with the transverse frequency have been ob-

tained. In the future we plan to further refine this analysis and check the scaling laws derived here against the predictions from other numerical codes. At high  $k_n$  the results observed for a sine-like (odd) perturbation of the type (2) are similar to the predictions for a cos-like (even) perturbation like (1). At low  $n$  the results are substantially different since the parity of the initial charge distribution plays a significant role. We plan to continue this study to the beam slice emittance, which is not affected by correlations between slices and is probably a better indicator of the influence of cathode inhomogeneities on the beam quality. This work will require a significant computational effort since the number of macroparticles and the transverse mesh fineness for the evaluation of the fields grow non-linearly with the frequency associated to the transverse mode.

## REFERENCES

- [1] L. Serafini, J.B. Rosenzweig, "Envelope analysis of intense relativistic quasilaminar beams in RF photoinjectors: a theory of emittance compensation" Phys. Rev. E55 (1997) p.7565.
- [2] L. Giannessi, M. Quattromini and C. Ronsivalle, "Emittance dilution due to 3D perturbations in RF-photoinjectors", Proceedings of 9<sup>th</sup> European Particle Accelerator Conference, 5 to 9 July, 2004, Lucerne, to be published.
- [3] L. Young, J. Billen "PARMELA" *LA-UR-96-1835*.
- [4] L. Giannessi, M. Quattromini, "TREDI simulations for high-brilliance photoinjectors and magnetic chicanes", PRST-AB 6 120101 (2003), Web site: <http://www.tredi.enea.it>.
- [5] AA.VV., LCLS Design Report, SLAC-R-593, April 2002.
- [6] C. Limborg et al. "Code comparison for simulations of photoinjectors ", Proceedings PAC2003.
- [7] M. Ferrario, private communication.
- [8] F. Ciocci et al., Nucl. Instr. and Meth. A393, (1997), 434.

# HARMONIC GENERATION AND LINEWIDTH NARROWING IN SEEDED FELS

L. Giannessi, ENEA Via E. Fermi 45, 00044, Frascati, Italy

## Abstract

The process of harmonic generation in a seeded, single pass, Free Electron Laser, are studied in the time/frequency domain following the evolution of the harmonics within a self consistent time dependent model. The first and second order correlation functions of the fundamental and of the higher order harmonics fields are studied as a function of the input seed amplitude.

## INTRODUCTION

Single pass Free Electron Lasers (FEL) operated in Self Amplified Spontaneous Emission (SASE) configuration are amplifiers of the natural shot noise of the driving electron beam. The spectral properties of the output radiation are the result of the amplification of the wide bandwidth noise arising from the stochastic distribution of the electron beam current, in the narrow bandwidth FEL amplifier. The properties of the output radiation, in terms of temporal coherence and intensity stability, have been extensively studied in literature [1][2][3] and reflect the stochastic nature of the electron beam shot noise. In a recent experiment at BNL[4] it has been shown that seeding a single pass FEL with an external laser allows to improve the spectral properties and the temporal stability of the laser source. In the same experiment it has been demonstrated that these properties are transferred to the higher order harmonics generated by the FEL. There is a widespread interest in this process, because emission on high order harmonics represents a significant resource to extend the wavelength tunability of an FEL and several recent proposals of FEL facilities rely on schemes based on seeding an harmonic generation[5]. The input seed, in order to be effective, must be characterized by enough intensity to overcome the intensity associated to the beam shot noise. The equivalent input intensity associated to a bunched beam is given by [6],

$$I_0 = \left\langle \exp(\zeta_i) \right\rangle^2 \frac{\rho P_e}{\Sigma_b} \quad (1)$$

where  $\Sigma_b$  is the electron beam cross section and  $P_e = I_{peak} m_0 c^2 \gamma / e_0$  is the e-beam peak power. The parameter

$$\rho = \frac{1}{2\gamma} \left( \frac{[\lambda_u K (J_0(\xi) - J_1(\xi))]^2}{4\pi \Sigma_b} \frac{I}{I_A} \right)^{\frac{1}{3}} \quad (2)$$

is the Pierce parameter, with  $\xi = K^2 / [4(1 + K^2/2)]$ , and  $\zeta_i = (k + k_u)z_i - \omega t + \varphi_{0,i}$  are the electron phases in the ponderomotive potential associated to an undulator of

period  $\lambda_u$  (with  $k_u = 2\pi/\lambda_u$ ) and strength  $K$ , and to an optical field  $E(z, t) = \tilde{E}(z, t) \exp(i(\omega t - kz))$ , being  $\tilde{E}(z, t)$  the slowly varying field component. In the specific case of randomly distributed electrons, the average  $\langle \exp(\zeta_i) \rangle$  is the normalized sum of  $n_e$  independent phasors, i.e.,

$$\left\langle \exp(\zeta_i) \right\rangle = 1 / \sqrt{n_e} \quad (3)$$

We estimate the number of interfering electrons  $n_e$  with the following naïve procedure. We define as

$$n_{1,e} = I_{peak} \lambda_0 / e_0 c \quad (4)$$

the number of electrons contained in a single resonant wavelength. Interference effects between electrons contained in contiguous wavelengths must be estimated. The field generated in a given longitudinal “slice” slips along the bunch and is amplified while the bunch travels along the undulator. This amplification must be considered in evaluating the interference between the fields emitted by electrons from different slices. The field evolution in presence of gain is given by [6],

$$\tilde{E}(z) = \frac{E_0}{3} \left[ e^{\left(\frac{i}{\sqrt{3}}+1\right)\frac{z}{2L_g}} + e^{\left(\frac{i}{\sqrt{3}}-1\right)\frac{z}{2L_g}} + e^{-i\frac{z}{\sqrt{3}L_g}} \right] \quad (5)$$

where  $L_g = \lambda_u / (4\pi\sqrt{3}\rho)$  is the FEL gain length. We can use eq. (5) as a function of the longitudinal coordinate, to weight the electron number in each slice. Adding up the weighted number of electrons contained in all the slices, in a portion of the bunch of length  $L\lambda_0/\lambda_u$ , we get

$$n_e = n_{1,e} \int_0^L |E_0 / \tilde{E}(z)| dz = f(L) I_{peak} L_g \lambda_0 / \lambda_u e_0 c \quad (6)$$

The dimensionless function  $f(L)$  grows linearly with  $L$  for the first gain lengths, then converges rapidly to the constant  $\sim 4.3$ . Assuming  $n_e \approx 4.3 I_{peak} L_g \lambda_0 / \lambda_u e_0 c$  as the total number of interfering electrons, we get from eq.(1)

$$I_0 \approx \lambda_u e_0 c / (4.3 I_{peak} L_g \lambda_0) \frac{\rho P_e}{\Sigma_b} \quad (7)$$

The equivalent input seed intensity  $I_0$  can be estimated more accurately by considering the gain length corrections associated to diffraction/inhomogeneous effects [8][9]. In this paper we will study with a time dependent numerical model, the coherence properties of

an FEL amplifier seeded with an input seed of amplitude varying across the “threshold” eq. (7).

## TEST CASES AND NUMERICAL MODEL DESCRIPTION

The analysis of longitudinal coherence in a single pass FEL amplifier has been developed by implementing a 1D time dependent model of an FEL amplifier in PERSEO [10]. PERSEO is a library of FEL dedicated functions available in the Mathcad environment. The basic element of PERSEO is a FEL pendulum-like equation solver for the particle dynamics, coupled with the field equations in the slowly varying envelope approximation (SVEA). The integrator includes self consistently the higher order harmonics. Transverse effects, as inhomogeneous broadening due to emittances, are accounted for by introducing an equivalent energy spread. In order to include time dependency, both the slowly varying field distribution and the electron phase space distributions are sampled longitudinally. At each time step the longitudinal slippage of radiation over the electron beam is applied shifting the radiation parameters array over the electron parameter arrays by an interpolation procedure. The implementation is capable of simulating the FEL interaction process for any profile of the input field/e-beam current, satisfying the SVEA approximation. In the cases studied, a continuous current distribution/input seed distribution, with a periodic boundary condition in the simulation window, has been considered. This choice allowed to minimize the number of parameters affecting the results. In table 1 the main simulation parameters are shown.

Table 1: Main simulation parameters.

Case label	A	B	C
$\lambda_0$ (nm)	50	15	5
Undulator K (peak)	2.2	2.2	2.2
Energy (MeV)	500	900	1550
En. spread (MeV)	0.4	0.4	0.4
$I_{\text{peak}}$ (A)	500	800	1500
N. emitt.(mm-mrad)	1	1	1
$\Sigma_b$ (mm <sup>2</sup> )	$3.2 \times 10^{-2}$	$1.8 \times 10^{-2}$	$1.04 \times 10^{-2}$
Pierce parameter $\rho$	$2.86 \times 10^{-3}$	$2.26 \times 10^{-3}$	$1.94 \times 10^{-3}$
$I_0$ , eq.(1) (W/cm <sup>2</sup> )	$4.4 \times 10^4$	$2.9 \times 10^5$	$1.9 \times 10^6$
Sim. window ( $\mu\text{m}$ )	250	200	200
Sampl. period ( $\mu\text{m}$ )	0.625	0.5	0.5
Sim. bandwidth	4%	1.5%	0.52%

We have selected three configurations with the operating wavelength in the VUV. This choice is driven by the general interest in seeding FELs with very high

order harmonics of the Ti-Sa laser, generated in gases[11]. These sources span the VUV region of the spectrum with a considerable level of peak power and constitute interesting candidates for seeding FEL amplifiers[5]. From the numerical representation point of view, at these wavelengths diffraction effects in the FEL dynamics are less severe. This mitigates the lack of accuracy due to the one dimensional FEL model implemented in PERSEO.

## RESULTS

The statistics of radiation and its coherence properties are studied with the first and second order correlation functions. In the time domain, the first order classical correlation function is defined by [12]

$$g_1(\tau) = \frac{\langle \tilde{E}(t) \tilde{E}^*(t + \tau) \rangle}{\sqrt{\langle |\tilde{E}(t)|^2 \rangle \langle |\tilde{E}(t + \tau)|^2 \rangle}} \quad (8)$$

An estimation of the coherence length can be obtained by the relation [12]

$$z_c = c \int_{-\infty}^{+\infty} |g_1(\tau)|^2 d\tau \quad (9)$$

In the hypothesis of a SASE FEL operating in the exponential growth regime, the coherence length (9) is a monotonic growing function of the longitudinal coordinate  $z$  in the undulator, and reads [3],

$$z_c = \frac{1}{6} \frac{\lambda_0}{\rho} \sqrt{\frac{z}{2\pi L_g}} \quad (10)$$

In fig.1, the coherence length evaluated according to eq.(10) has been compared with the values calculated from the simulation data,

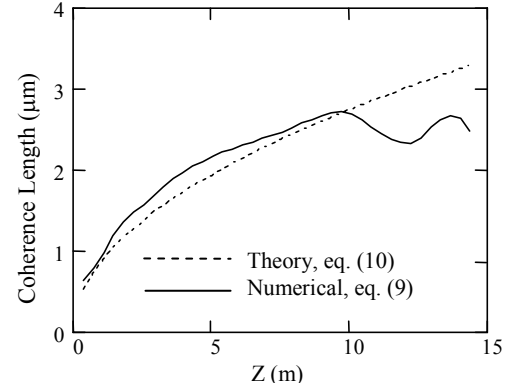


Fig. 1. Coherence length as given by eq. (10) (dashed line) and as calculated from the simulation data, according to eq.(9) (continuous line)

The plot in fig. 1 has been obtained simulating the configuration in column A of table 1, starting from the natural shot noise (no input seed). The beam energy spread has been set to zero in order to preserve the homogeneous conditions in which eq.(10) has been

derived. The agreement is reasonable until saturation, which is occurring at  $z \sim 10\text{m}$ , is reached.

In fig. 2 the growth of the laser intensity as a function of the longitudinal coordinate is shown. The parameters are those of tab.1, col. *A*, with an input seed represented by a perfectly uniform classical wave of intensity  $I_s = 3.1 \times 10^5 \text{ W/cm}^2$ .

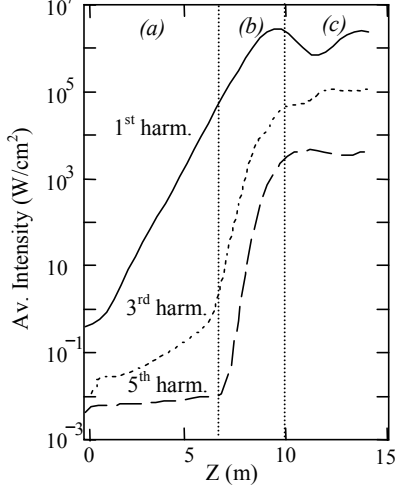


Fig. 2. Laser intensity vs. the longitudinal coordinate for the first three odd harmonics. The regions of exponential growth (*a*), harmonics generation (*b*) and saturation (*c*) have been indicated in the figure.

In fig. 2 we can distinguish the region, labeled with (*b*), where the growth of the third/fifth harmonic intensity is driven by the beam bunching due to the ponderomotive potential relevant to the first harmonic field.

The typical spectra for the third harmonic field, as calculated in regions (*a*) and (*b*) are shown in figs. 3.a,b respectively. In fig. 3.a the third harmonic field is not yet locked in phase to the bunching induced by the fundamental. The situation changes in fig. 3.b, where the phase of the third harmonic field is determined by the bunching on the fundamental and the coherence properties of the seed are transferred to the third harmonic. A similar behaviour is observed for the fifth harmonic.

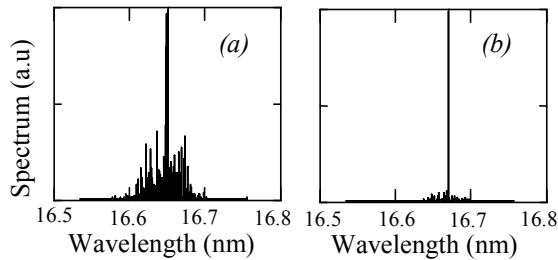


Fig.3. Third harmonic spectrum in the region (*a*) (at  $z \sim 4.7\text{m}$ ) and in the region (*b*) (at  $z \sim 7.2\text{m}$ ). The relative r.m.s. linewidth is  $\sim 0.174\%$  in (*a*) and  $\sim 0.076\%$  in (*b*).

In fig.4 it is shown the behaviour of the maximum coherence length reached along the undulator, as a function of the input seed intensity. The parameters are

those of table 1, column *A*. At  $500\mu\text{m}$  the coherence length saturates because of the limited extension of the simulation window ( $250\mu\text{m}$ ). The value of the intensity calculated according to eq.(1) is shown as a vertical dashed line. In figs. 5 and 6 are shown the equivalent plots obtained with the parameters listed in columns *B* and *C* of table 1 respectively.

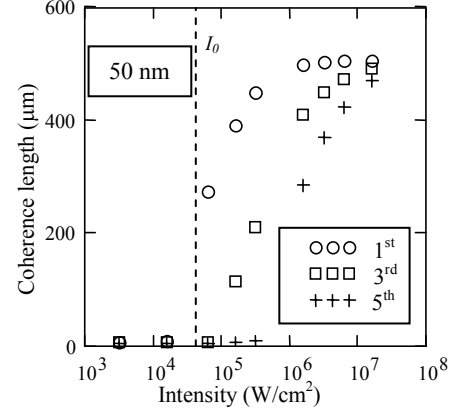


Fig. 4. Maximum coherence length reached along the undulator, as a function of the input seed intensity in the test case *A*. The dashed line indicates the threshold intensity  $I_0$  evaluated according to eq. (7).

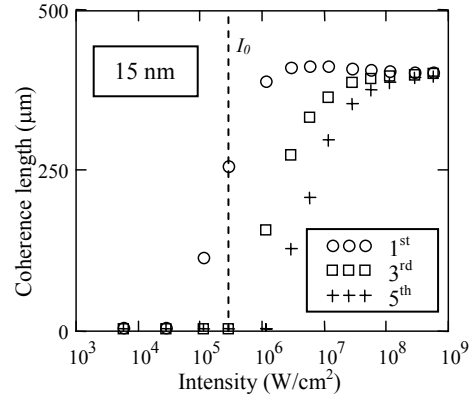


Fig. 5. As in fig.4 with the parameters of tab.1, col. *B*.

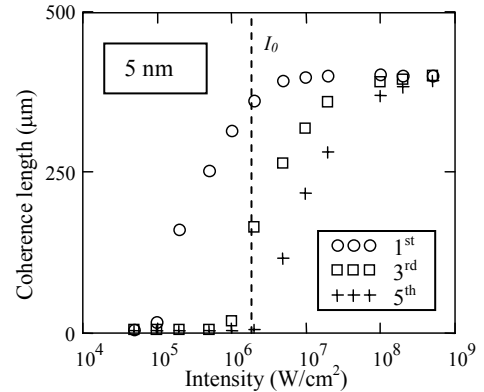


Fig. 6. As in fig.4 with the parameters of tab.1, col. *C*

As expected the power level required to ensure coherence on the higher order harmonics grows with the harmonic order. Comparing figs. 4, 5 and 6 it appears that the equivalent seed  $I_0$  obtained according to eq.(7),

slightly overestimates the intensity required to establish coherence on the fundamental harmonic, as the wavelength decreases (parameters of col. C, fig.6). It must be stressed that the intensity of eq.(1) still matches quite well the intensity that can be obtained by extrapolating the laser intensity at  $z=0$  from the simulation data.

The intensity fluctuations have been studied calculating the second order correlation function  $g_2(\tau)$  [12]:

$$g_2(\tau) = \frac{\langle |\tilde{E}(t)|^2 |\tilde{E}(t+\tau)|^2 \rangle}{\langle |\tilde{E}(t)|^2 \rangle \langle |\tilde{E}(t+\tau)|^2 \rangle} \quad (11)$$

as a function of the longitudinal coordinate along the undulator. From the definition (11), and assuming  $I(t) \propto |\tilde{E}(t)|^2$ , it follows that

$$\sqrt{g_2(0)-1} = [I/\langle I \rangle]_{RMS} \quad (12)$$

In figs.7, 8 and 9 it is shown the minimum along the undulator of the r.m.s. intensity (12), as a function of the seed intensity, in the cases *A*, *B* and *C* respectively. The averages in (12) are taken over the temporal extension of simulation window.

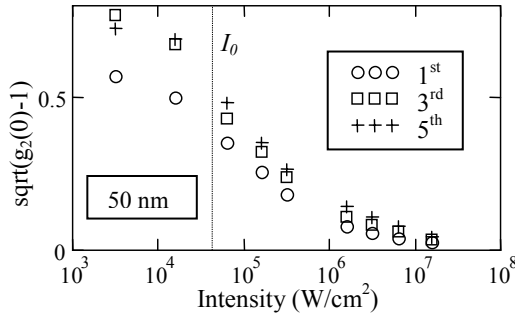


Fig. 7. Standard deviation of the intensity fluctuations vs. the seed intensity with the parameters of tab.1, col. A

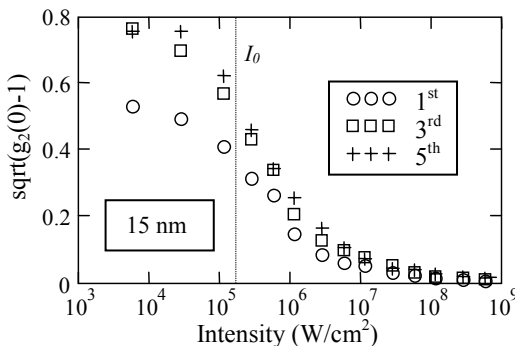


Fig. 8 As in fig. 7, with the parameters of tab.1, col. B

In a SASE FEL in the exponential growth regime, we have  $\sqrt{g_2(0)-1} = 1$  [3]. As expected the effect of the seed is that of suppressing the intensity fluctuations but this

transition is smoother than the one observed in establishing the temporal coherence (figs. 4,5 and 6).

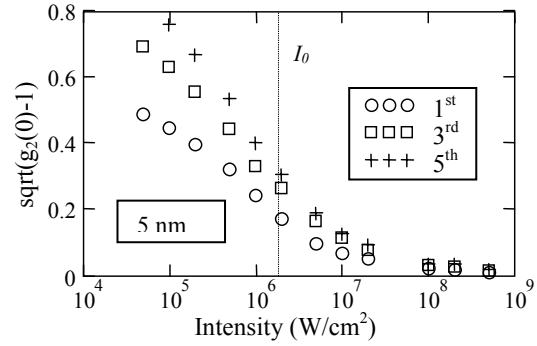


Fig. 9. As in figs. 7,8 with the parameters of tab.1, col. C

Fluctuations of the higher order harmonics are larger than fluctuations on the fundamental. The amplitude of the seed required for suppressing the fluctuations exceeds by orders of magnitude the intensity provided by eq.(7).

## CONCLUSIONS

We have analysed the coherence properties of a seeded FEL amplifier as a function of the seed amplitude. The equivalent intensity associated to the beam shot noise, eq.(7), has been compared to the transition to coherence induced by the presence of a seed. The results obtained so far constitute a preliminary analysis which gives an indication about the power requirements of the input seed, in order to be effective in improving the coherence properties of a single pass FEL.

## REFERENCES

- [1] R. Bonifacio, L. De Salvo, P. Pierini, N. Piovella, C. Pellegrini, Phys. Rev. Lett. 73 (1994) 70 and references therein.
- [2] P. Pierini, W. M. Fawley, Nucl. Instrum. & Meth. A 375 (1996) 332-335
- [3] E.L. Saldin, E.A. Schneidmiller, M.V. Yurkov, Optics Communications 148, (1998) 383-403
- [4] L. H. Yu et al., Phys. Rev. Lett. 91 (2003) 74801
- [5] Workshop on the Physics of Seeded Free Electron Lasers, 17-19 June 2004, MIT campus, Cambridge, MA <http://mitbates.mit.edu/xfel/conference.htm>
- [6] G. Dattoli, P.L. Ottaviani, Journal of Appl. Phys. 86 (1999) 5331
- [7] See e.g. G. Dattoli, A. Renieri, A. Torre, Lectures on the Free Electron Laser Theory, World Scientific ed. (1993) p. 493
- [8] M. Xie, in *Proceedings of the Particle Accelerator Conference, Dallas, TX, 1995* (IEEE, Piscataway, NJ, 1996), p. 183. Sect. A **483**, 101 (2002).
- [9] G. Dattoli, L. Giannessi, P.L. Ottaviani, C. Ronsivalle, Journal of Appl. Phys. 95 (2004) 3206
- [10] <http://www.enea.perseo.it>
- [11] P. Salières et al., Science **292** (2001) 902
- [12] See e.g. R. Loudon, Quantum Theory of Light, Oxford Univ. Press (2000), chapter 3.

# SEEDING HIGH GAIN HARMONIC GENERATION WITH LASER HARMONICS PRODUCED IN GASES

G. Lambert\*, B. Carré, M. E. Couprie, D. Garzella, Y. Mairesse, P. Salières, CEA, DSM/SPAM, 91 191 Gif-sur-Yvette, France, A. Doria, L. Giannessi, ENEA C.R. Frascati, Italy, T. Hara, H. Kitamura, T. Shintake, SPring-8/RIKEN Harima Institute, Hyogo 679-5148, Japan

## Abstract

Free electron Lasers employing High Gain Harmonic generation (HG) schemes are very promising coherent light sources in the soft X-ray range. They offer both transverse and longitudinal coherence, while Self Amplified Spontaneous Emission schemes have a limited longitudinal coherence. We propose here to seed a HG experimental setup with high harmonics produced by a Ti:Sa femtosecond laser focused on a gas jet in the 100-10 nm spectral region. The implementation of this particular laser harmonics source as a seed for HG is investigated. Semi analytical and numerical 1D calculations are given, for the cases of the SCSS, SPARC and ARC-EN-CIEL projects.

## INTRODUCTION

In order to reach very short wavelengths in systems based on Free Electrons Laser (FEL) [1,2], and to have more compact and fully temporally coherent sources, a High Gain Harmonics Generation (HG) configuration [3] is studied here, in which an external laser source is seeded into a modulator, thus allowing a strong prebunching of the e-beam. The use of a long radiator section can lead to the consistent emission of radiation at high order harmonics of the seeding source while reproducing its longitudinal and transverse coherence. A very promising scheme is the one where the seeding source is already in the XUV range, provided by the harmonics of the Ti:Sa laser generated in gas. Intense, ultra-short laser harmonics can be now generated down to 10 nm [4]. We propose to use these laser High Harmonics (HH at  $\lambda$  wavelength) as the seed for a high gain FEL amplifier radiating at  $\lambda$  or  $\lambda/3$  and to extract its third and fifth non linear harmonics [2,5]. This scheme is considered for different installations: first on SCSS (Spring-8 Compact Sase Source, Japan) [6] and SPARC (Sorgente Pulsata e Amplificata di Radiazione Coerente, Italy) [7] for demonstration experiments, second on ARC-EN-CIEL (Accelerator-Radiation Complex for ENhanced Coherent Intense Extended Light, France) [8] and BATES (MIT, USA) [9] for efficient X-ray generation. SCSS and SPARC are projects of linac-based FEL, providing a compact SASE source with high brightness in the X-ray range. ARC-EN-CIEL (AEC) is a proposal for an innovative HG in the XUV range (Phase 1 is a first step towards VUV). In this paper, we discuss the prototype experiments on SCSS, AEC and SPARC, including a brief description of the experimental setup and theoretical estimate of the performances, the latter

\*[guillaume.lambert@lure.u-psud.fr](mailto:guillaume.lambert@lure.u-psud.fr)

based on analytical formulae [1, 10] and 1D simulations using PERSEO code [11].

## THEORY OF HIGH ORDER HARMONICS PRODUCED IN GASES

The high harmonic generation in rare gas (Xe, Ar, Ne, He) results from the strong non linear polarisation induced by the strong laser field  $E_{\text{Laser}}$ , at intensity  $10^{14}$ - $10^{15}$  W/cm<sup>2</sup>. The process is qualitatively described in the semi-classical “three-step” model [12, 13]. Close to laser focus, for  $E_{\text{Laser}}$  comparable to the intra-atomic field, atoms ionize in the tunnelling regime [4] (step 1). The ejected electrons are then accelerated by the laser field and gain a kinetic energy (step 2). Those which are driven back close to the core may recombine to the ground state, emitting a burst of XUV photons (step 3). This three-step process reproduces every half-optical cycle.

## EXPERIMENTAL SET UP

### Characteristics of High Harmonics in gases

A typical harmonic spectrum generated in Ne is displayed in fig. 1, illustrating the characteristic distribution of the odd harmonics into the “plateau” region, where the conversion efficiency is almost constant, and the “cut-off” region where the conversion efficiency rapidly drops down. The conversion efficiency for high harmonic (HH) generation remains relatively weak, typically varying from  $10^{-4}$  in the plateau to  $10^{-7}$  in the cut-off.

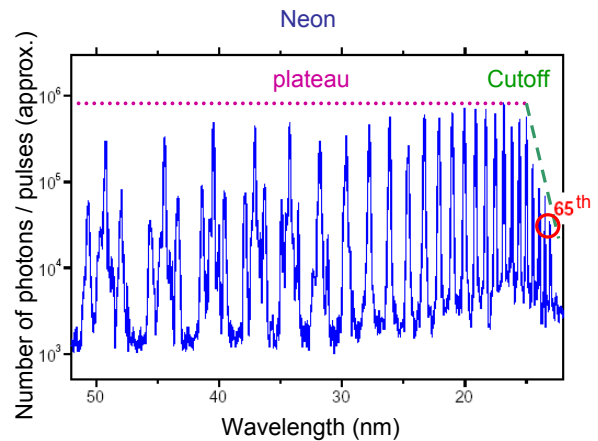


Fig. 1: High Harmonic spectrum in Ne.

The upper spectral limit is given by the “cut-off law” [5, 14]. It states that the lighter the gas, i.e. the higher the ionization potential and the laser intensity to which atom

can be submitted without ionizing, the higher the cut-off energy. The HH therefore cover the  $100^{-3}$  nm range (12-400 eV). They have remarkable properties of ultra-short duration (of a few 10 fs down to sub-fs), longitudinal [15] and transverse [16] coherence, good beam quality (small divergence  $\sim 1$  mrad on laser axis), easily rotatable linear polarization [17] and can be produced at relatively high repetition rate (up to KHz). Finally it is possible to continuously tune the HH, e.g. by manipulating the spectral phase of the driving laser or by starting from two driving frequencies [18].

### Beams and undulators parameters

For the seed experiment, a HGHG configuration is foreseen with two undulators: the modulator (mod), which is chosen according to the wavelength of the seeded radiation, and the "radiator" (rad), providing a high gain. In SCSS and SPARC projects, the radiator emitted wavelength is matched on the fundamental of the modulator ( $\lambda_{\text{rad}} = \lambda_{\text{seed}}$ ). In AEC and AEC Phase 1 projects it is matched on the third harmonic ( $\lambda_{\text{rad}} = \lambda_{\text{seed}}/3$ ). The table 1 shows the electron beam parameters, where  $I_p$  is the peak current, the undulators parameters, where  $N_p$  is the number of periods per section and  $N_s$  the number of section, and the seeding parameters, where  $E_H$  is the harmonic energy per pulse,  $P_H$  the harmonic power and  $D$  the harmonic spot diameter.

Table 1: electron beam, undulator, and seeding characteristics.

Projects	AEC PhI	AEC	SCSS	SPARC
Electron Beam Characteristics				
E (GeV)	0.22	1	0.25	0.21
$\sigma_\gamma$	0.001	0.001	0.0002	0.002
Q (nC)	1	1	1	1
$\varepsilon$ ( $\pi$ mm-mrad)	1.7	1.5-2	1.5	1
$I_p$ (kA)	0.8	0.6	0.2	0.15
Undulators Characteristics (Mod/Rad)				
$\lambda_R$ (nm)	267/89	14/4.64	60	160
$\lambda_U$ (nm)	38.9/20	30/20	15	28
K	1.76/1.14	2.27/1.26	1.39	1.36
$N_p$	34/450	160/1000	300	487
$N_s$	1/1	1/1	2	6
Seeding Characteristics				
$\lambda_{\text{seed}}$ (nm)	H3=267	H57=14	H13=60	H5=160
$E_H$ ( $\mu$ J)	5	1	5	5
$P_H$ (MW)	50	10	50	50
D ( $\mu$ m)	250	250	250	250

### Layout of the HGHG configuration seeded by harmonics produced in gases

A Ti:Sa laser system delivers pulses at 800 nm ( $E_{\text{ph}}=1.55\text{eV}$ ), which are converted into harmonics in the gas jet vessel. The harmonic pulses are then injected into the modulator. In SCSS and ARC-EN-CIEL projects, a

magnetic chicane is inserted on the electron bunch path to superimpose the bunch and the XUV pulse at entrance of the modulator (Fig. 1).

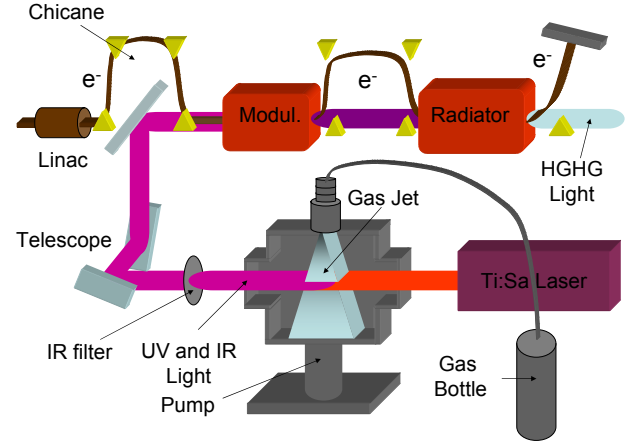


Fig. 1: Layout of the seeding system with a chicane.

A small size mirror serves to inject the XUV beam in the FEL cavity and to adjust its position. The advantage in this scheme is that all the XUV beam ( $\sim$ mm in diameter) is injected; the constraint is that enough room should be available to accommodate the magnetic elements. So, another arrangement, where the chicane is replaced by a holed mirror on the XUV beam, is envisaged in the SPARC project (Fig. 2).

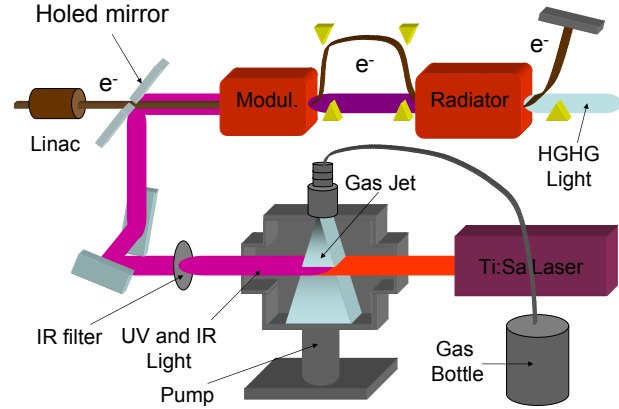


Fig. 2 : Layout of the seeding system with a holed mirror.

The constraint is now that the hole should be sufficiently small so that a high enough XUV energy is reflected.

In both schemes, the laser beam is eliminated using various metallic filters which further select a finite spectral range in the harmonic spectrum. Then the XUV beam should be collimated to a small diameter (mm) by means of a telescope (spherical mirrors in afocal geometry). The different mirrors should also improve, if needed, the spectral selection of a particular harmonic component, e.g. Mo/Si multilayer optics to select high orders in SCSS [19, 20]. The required multiple reflections should not reduce the XUV energy by more than 50%. Thus, if we consider a harmonics injection system based on five optics the global reflectivity falls around 3%.

## CODES AND SIMULATIONS

### One dimensional code PERSEO

Perseo [11] is a library of functions reproducing the main properties of the desired FEL configuration in a 1D simulation. The basic idea consists in the integration of the pendulum equation coupled to the fields equations. A typical simulation is shown in fig. 4.a,b where the growth of the output peak power on the fundamental and on the higher order non-linear harmonics is represented as function of the longitudinal coordinate in the radiator. The implementation of Perseo considered in this study allows to inspect the energy modulation (fig. 5a) and the associated bunching factor evolution (fig. 5b), during the parameters optimization. Finally in fig.6, the evolution of the output peak power on the harmonics is shown as a function of the seed power and the radiator length.

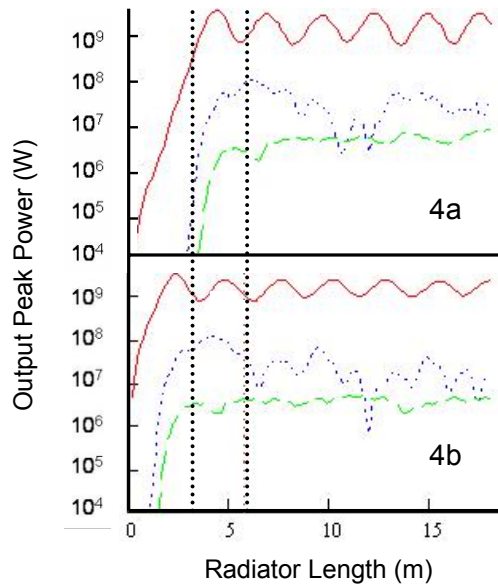


Fig. 4a, 4b: Evolution of the AEC SASE (a) and AEC Seeding HGHG (b) output peak power at 6.5nm (—) and at their third (...) and fifth (---) non linear harmonics.

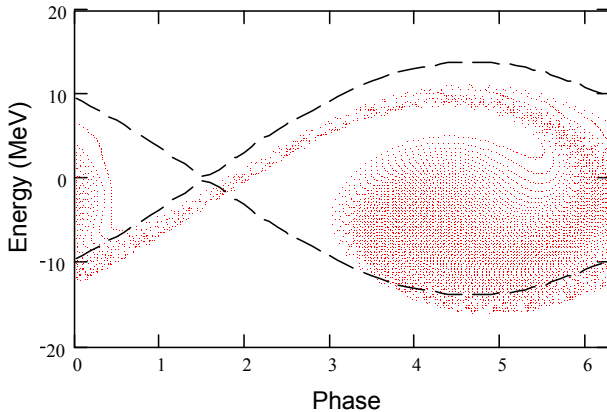


Fig. 5a: Evolution of the energy modulation before the drift section for SPARC project.

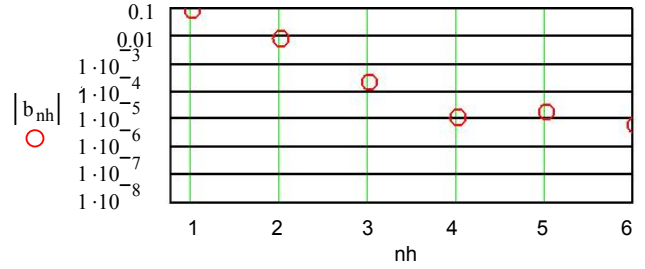


Fig. 5b: Evolution of the harmonics bunching factor ( $b_{nh}$ ) before the drift section for SPARC project versus the order of harmonics ( $nh=1$  is the fundamental).

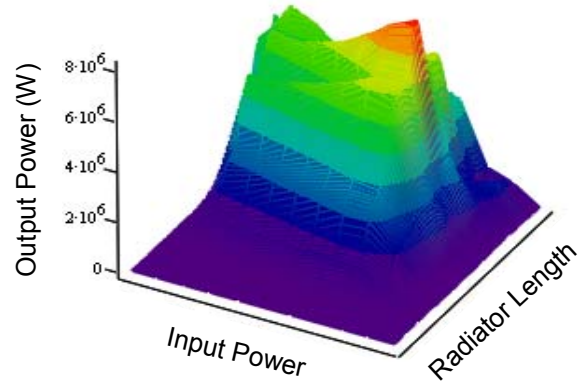


Fig. 6: Evolution of the SPARC Seeding HGHG output peak power for the third non linear harmonics (53.3 nm) versus input power and radiator length.

### Analytical simulation

These simulations are based on an analytical 0D approach in static mode, that is to say, with an average on the transverse and longitudinal coordinates. The used FEL formula come from G. Dattoli and P. L. Ottaviani [10]. The simulations allow to investigate the exponential growth of the fundamental output peak power as a function of the radiator length.

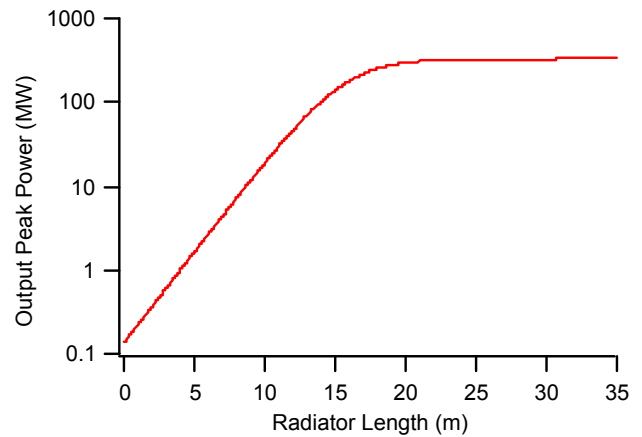


Fig. 7: Evolution of the AEC Seeding HGHG output peak power at 6.5nm.

## EXPECTED PERFORMANCES

We can see in table 2 that seeding HGHG configuration allows the saturations lengths to be reduced from a factor of 1.5 to 2.

Table 2: Saturation length (m) comparison with Perseo: Seeding HGHG/SASE.

Projects	Fundamental Output Radiation (nm)	Saturation Length (Seeding/SASE) (m)
ARC-EN-CIEL	9.2	2/7.5
	6.5	3.5/7.5
	5.5	7/12
ARC-EN-CIEL Phase 1	88.9	3.5/5.5
	66.7	4.5/7
	53	6/12
SCSS	60	4/7.5
SPARC	260	4/6
	160	6/8.5

Figure 8 shows the expected results in terms of output power made with Perseo.

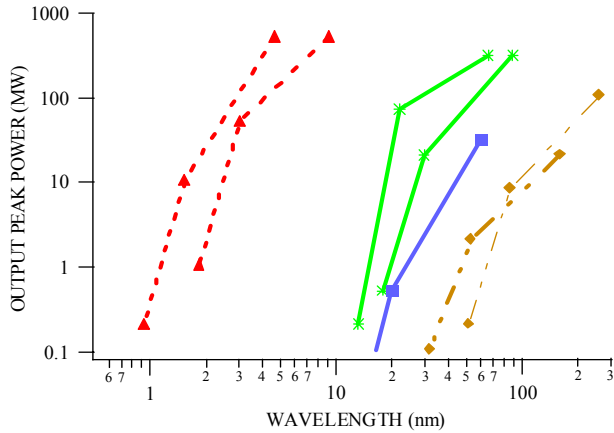


Fig. 8: Output peak power of  $\lambda_{\text{rad}}$ , its third and fifth non-linear harmonics for AEC (-- $\blacktriangle$ --), AEC phase 1 (-\*-), SCSS (- $\blacksquare$ -), SPARC (- $\blacklozenge$ -), and, for seed powers up to 1MW.  $\langle P_{\text{Rad}} \rangle \approx 0.1-0.5$  W.

As we can see on the figure 4a and 4b, the output peak power is lower by a factor of  $\sim 5$  for a Seeding HGHG configuration than for a SASE configuration. However, it remains high and now corresponds to fully coherent XUV pulses. For instance, if we seed the SPARC experiment at 260 nm, the fifth harmonic at 52 nm is generated at 0.25 MW output level, whereas seeding at 160 nm gives a fifth harmonic at 32 nm of 0.15 MW peak power.

Figure 9 shows the expected results in terms of output power obtained by the analytical simulations.

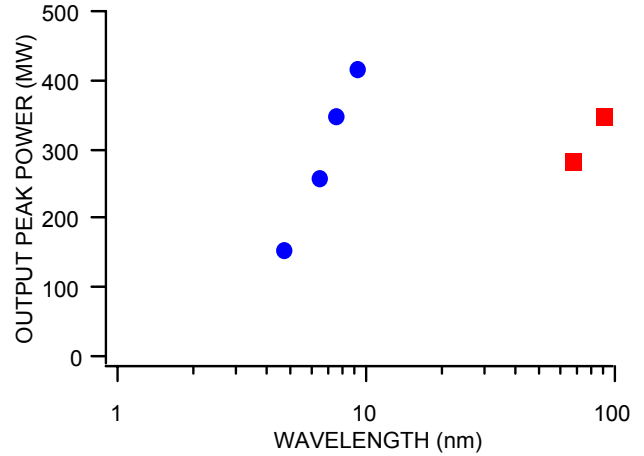


Fig. 9: Output peak power of the  $\lambda_{\text{seed}}/3$  harmonics performances with a 1MW seed power and with beam parameters coming from Table 1, for AEC ( $\bullet$ ), and AEC phase 1 ( $\blacksquare$ ).  $\langle P_{\text{seed}} \rangle \approx 0.1-0.5$  W.

## CONCLUSIONS

Using high laser harmonics generated in gas for seeding High Gain FEL amplifiers appears very interesting, since the seed radiation is fully coherent, of ultra-short duration and tuneable in the XUV range. The seeding can reduce the saturation length, leading to a more compact source. The calculated performances roughly agree between 0 and 1D analysis. They show that high peak power ( $> \text{MW}$ ) could be obtained with this scheme.

## REFERENCES

- [1] F. Ciocci et al, IEEE Jour. Quant. Elec. 31 (1995) 1242.
- [2] S. G. Biedron et al., Nucl. Inst. Meth. A 475 (2001) 401.
- [3] L. H. Yu, I. Ben-Zvi, Nucl. Inst. Meth. A 393 (1997) 96.
- [4] K. Midorikawa, Phys. Rev. Lett. 82 (1999) 1422.
- [5] D. Garzella et al., Nucl. Inst. Meth. A 527 (2004).
- [6] <http://www-xfel.spring8.or.jp/scss/>.
- [7] Sparc Collaboration, Nucl. Inst. Meth. A 507 (2003) 345.
- [8] ARC-EN-CIEL [www.lure.u-psud.fr/congres/femto/](http://www.lure.u-psud.fr/congres/femto/).
- [9] <http://mitbates.mit.edu/xfel/>.
- [10] G. Dattoli, P. L. Ottaviani J. Appl. Phys., 95, (2004).
- [11] [www.perseo.enea.it](http://www.perseo.enea.it).
- [12] P. B. Corkum, Phys. Rev. Lett. 71 (1993) 1994.
- [13] M. Lewenstein et al., Phys. Rev. A 49 (1994) 2117.
- [14] G. Lambert et al., to be published in Jacow.
- [15] P. Salières et al., Science 292 (2001) 902.
- [16] L. Le Déroff et al., Phys. Rev. A 61 (2000) 043802.
- [17] P. Salières et al., Adv. At., Mol., Opt. Phys. 41 (1999) 83.
- [18] H. Eichmann et al., Phys. Rev. A 51 (1995) R3414.
- [19] Yu. A. Uspenskii, Nucl. Inst. Meth. A448 (2000) 147.
- [20] T. Feigl et al., Nucl. Inst. Me